Available online at www.sciencedirect.com

ScienceDirect

journal homepage: www.elsevier.com/locate/he

Synthesis, characterizations, and hydrogen sulfide gas sensing application of BiO_x (x = 1, 1.5) nanostructures

Krishna D. Bhalerao [a,1], Yogesh T. Nakate [b,c,**], Sandip P. Choudhury [d,***], Umesh T. Nakate [e,*], M.A. Yewale [f,1], S.L. Kadam [g], R.S. Ingole [h], S.C. Kulkarni [i], Y.B. Khollam [j]

[a] School of Chemical Science, Kavayitri Bahinabai Chaudhari North Maharashtra (KBCNM) University, Jalgaon, 425001, Maharashtra, India

[b] Department of Electronics, Kavayitri Bahinabai Chaudhari North Maharashtra (KBCNM) University, Jalgaon, 425001, Maharashtra, India

[c] Department of Electronics, Yeshwant Mahavidyalaya, Nanded, Maharashtra, India

[d] Amity School of Applied Science, Amity University, Jaipur, Rajasthan – 303002, India

[e] Department Polymer Nano Science and Technology, Jeonbuk National University, Jeonju-si, Jeollabuk-do, Republic of Korea

[f] School of Mechanical Engineering, Yeungnam University, Gyeongsan, 38541, Republic of Korea

[g] Department of Materials Science and Engineering, Seoul National University, Seoul, Republic of Korea

[h] Graduate School of Energy Science and Technology (GEST), Chungnam National University (CNU), Daehak-ro, Yuseong-gu, Daejeon, 34134, South Korea

[i] Department of Electronic Science, M. S. G. Arts, Science, and Comm. College Malegaon-Camp (Nashik), Savitribai Phule Pune University, MS 423105, India

[j] Department of Physics, Baburaoji Gholap College, Pune, Maharashtra, India

HIGHLIGHTS

- 2D Nanosheets structured BiO_x *via* hydrothermal technique and characterizations.
- BiO_x sensor exhibiting high response and good selectivity towards H_2S gas at 250 °C.
- BiO_x sensor highly sensed in H_2S gas concentration 10–100 ppm at 250 °C.
- BiO_x sensor shows dynamic sensor resistance response with excellent repeatability.
- BiO_x sensor shows long term stability.

GRAPHICAL ABSTRACT

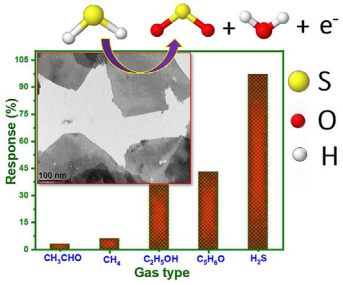

* Corresponding author.
** Corresponding author.
*** Corresponding author.
E-mail addresses: yogesh.nakate@gmail.com (Y.T. Nakate), sandip.pchoudhury@gmail.com (S.P. Choudhury), umesh.nakate@gmail.com, umesh.nakate@jbnu.ac.kr (U.T. Nakate).

[1] Represents the equal contribution.

https://doi.org/10.1016/j.ijhydene.2022.09.235

ARTICLE INFO

Article history:
Received 28 June 2022
Received in revised form
19 September 2022
Accepted 24 September 2022
Available online 14 October 2022

Keywords:
Hydrothermal synthesis
Bismuth oxide
Nanosheets
Hydrogen sulfide
Gas sensor

ABSTRACT

Hydrogen sulfide is one of the harmful gases that contribute to air pollution. Therefore, there is a need to develop high-response hydrogen sulfide (H_2S) gas sensors. Herein, the bismuth oxide nanostructured material was prepared using the hydrothermal chemical route. The prepared material was characterized using XRD, FESEM, TEM, XPS, EDS, and UV–visible spectroscopy techniques. The gas sensor device was fabricated using bismuth oxide nanomaterial, and gas sensing properties were investigated. The sensor exhibited the highest response of 22–92% towards H_2S gas at 250 °C for 10–100 ppm concentration range, respectively. The 92% response was recorded for 100 ppm H_2S gas with rapid response and recovery times of 511 and 492 s, respectively. The sensor was tested at different operating temperatures and H_2S gas concentrations. The sensor's selectivity, dynamic resistance response repeatability, and long-term (30 days) stability were studied. The nanostructured bismuth oxide can be a promising candidate for high-response H_2S sensor applications.

Introduction

Gas sensors are essential and undeniable devices in the modern world; they are primarily used in pollution monitoring, public safety, quality control, air quality analysis, agriculture technologies, chemical industries, and so on. The human sense of smell is susceptible to detecting and discriminating gases or odors at low concentrations [1]. Most poisonous gases or harmful vapors are only detectable at high concentrations [2]. High-performance gas chromatography [3] and ion-chromatography [4] own higher responses for lower gas and vapor concentrations. However, these chemical methods are expensive and require more processing. Thus, chemical techniques may not be followed for environmental air monitoring (EAM), and therefore it is an urgent need to develop fast, portable, and cost-effective sensor devices for EAM.

Among all the sensing materials investigated so far, metal oxides (MOs) are the most famous for detecting harmful gases. More than 150 gases have been analyzed using metal oxides, and most commercial sensors are made from metal oxide [5]. The success is due to its advantages, such as simple design, rapid response time, high sensitivity, compact size, and low cost [6]. n-type semiconducting materials are favorable in gas sensor applications. They are more thermally and chemically stable to detect harmful gases. Therefore, researchers need to develop gas sensor devices with good sensing ability and a high response rate. Furthermore, some of the most toxic gases are reductive when they interact with n-type material, decreasing their resistance.

The present work focuses on hydrogen sulfide (H_2S) sensing using the conductometric method. H_2S, also known as manure gas, is highly toxic and flammable [7]. It commonly occurs in sewer lines, geothermal plants, and more than 70 types of industries that produce this gas as a by-product [8]. It has severe effects on the human body; hence detection of such gas is very much important. So far, many metal oxides have been studied for the detection of H_2S gas. Transitional metal oxide-based nanostructures such as SnO_2, ZnO, CuO, Fe_2O_3, and WO_3 have been reported over the years for gas sensing applications [9–13]. Among semiconducting metal oxide sensing materials, bismuth-based sensors are relatively less focused. There are reports on bismuth-based oxide nanostructured materials reported for hydrogen sulfide gas sensing which suggest that bismuth-based oxide materials have the potential to exhibit high-performance hydrogen sulfide sensor applications [14,15]. The remarkable properties of nanostructured bismuth oxide made it the potential sensor material. Bismuth oxide, one of the important transition metal oxides, is non-toxic, environmentally friendly, has good conductivity, is readily available, and is a low-cost material. In addition to this, it has five polymorphs *i.e.* α, β, χ, δ, and ε, in different nanostructures. In the present work, the novel ultrathin nanosheet structures of BiO_x with different stochiometry (different oxygen composition) were synthesized using the versatile hydrothermal chemical method. Hydrothermal synthesis is a simple and ultrafast chemical method that has been used in literature to obtain nanostructures of different metal oxides [13]. The hydrothermal synthesis route has several advantages such as easy to scale up (high yield), controlled shape and size, easy operation, affordable (cheap), *etc* as compared to other established methods [16]. Further, characterizations were performed using sophisticated instruments *viz* XRD, FESEM, TEM, EDS, UV–Visible spectroscopy, and XPS. Structural parameters of BiO_x nanosheets material were estimated by XRD analysis. Resistance variation of BiO_x nanosheets sensor as a function of different gas concentrations and temperatures were recorded. The selectivity and stability studies were carried out. The sensor's performance is compared with reported H_2S sensor data.

Experimental

The BiO_x nanopowder was synthesized using an easy hydrothermal chemical route. For this, bismuth nitrate (0.005 M) and Na_2SO_4 (0.05 M) were dissolved in 60 ml of de-ionized (DI) water. An aqueous sodium hydroxide of 0.045 M solution was

prepared and added to the previous solution dropwise and kept stirring at 1200 rpm. This prepared solution was transferred into an autoclave (Teflon-lined) and sealed it in a steel case, and put in an electric oven at 150 °C for up to 12 h. The obtained precipitate was washed using DI water and ethanol multiple times. The final solid product was dried overnight at 70 °C temperature and crushed, followed by air annealing at 400 °C in a muffle furnace for 2 h to remove impurities and achieve crystallinity.

The drop-casting technique was used to fabricate the BiO_x sensor [17]. Initially, BiO_x nanopowder obtained from hydrothermal synthesis was mixed into ethylene glycol in the appropriate amount and formed a uniformly dispersed solution using ultrasonication for 15 min. An alumina substrate having an inter-digital pattern (IDT) of Pt was cleaned thoroughly. Two external wires (Au coated) were connected to the terminals of the IDT pattern using gold paste for electrical contacts. A picture of the sensor device is shown in Scheme 1. Then with the help of a micropipette, the prepared active material solution was cast on a platinum electrode pattern of the area of 1 cm^2. Finally, the drop cast sensor device was annealed at 300 °C in order to remove the ethylene glycol and achieve a uniform sensor film. Gas sensor testing was carried out using a fully automated gas sensing unit where we have a mass flow meter to control the airflow along with a Keithley electrometer and data acquisition software installed computer. The schematic of the testing setup is shown in Scheme 1. The formula for the response calculation is represented in Eq. (1) [18].

$$S(\%) = \frac{Ra - Rg}{Ra} X\ 100 \quad (1)$$

where S represents the response, R_a and R_g are the stabilized resistances of the sensor in air and target gas, respectively. Senor measurement was carried out in a fully automated gas sensor assembly where a mass flow controller (MFC) was used to inject the carrier gas. The data acquisition was done over the computer interfaced with the Keithley electrometer.

Results and discussion

Structural properties

The XRD is a primary standard tool to determine the crystal structure and confirm any specific crystalline material. The XRD pattern for as-prepared materials was recorded at normal room temperature and pressure conditions at the diffraction angle of 20–90° using an X-ray diffractometer machine. Fig. 1 shows the XRD pattern, along with standard line spectra from JCPDS data for the obtained material. The intense and sharp diffraction peaks were observed that confirm the highly crystalline nature of the prepared material. The characteristics XRD peaks were matched for two different phases *viz* $BiO_{1.5}$ and BiO. The highest intense XRD peak matches with (111) plane, and the low intense XRD peak corresponds with the (222) plane of cubic structured $BiO_{1.5}$ compound as per JCPDS#78–0736. The three average intensity XRD peaks were matched with the (012), (104), and (015) planes, confirming the presence of hexagonal structured BiO compound as per JCPDS#75–0995.

Morphology and elemental analysis

The as-prepared BiO_x material was employed for FESEM and TEM analysis to investigate the shape, surface texture, and size of particles. The FESEM image of BiO_x powder is depicted

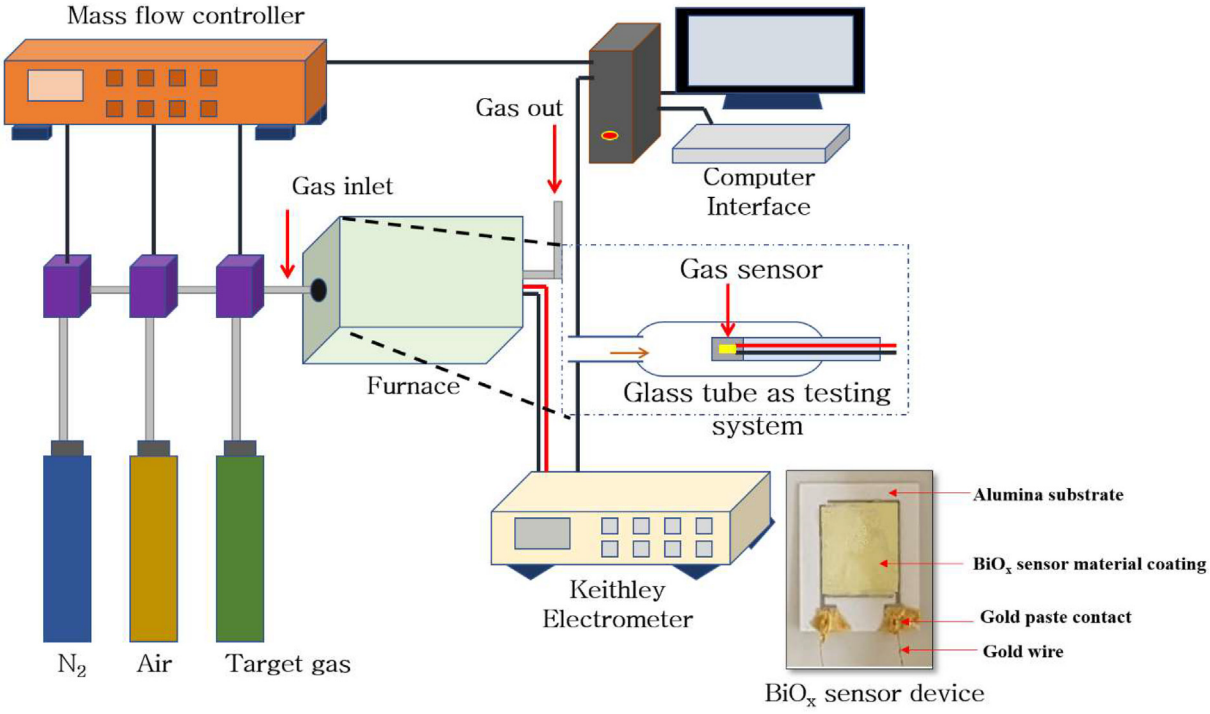

Scheme 1 – Schematic of experimental sensing test setup and picture of BiO_x sensor device.

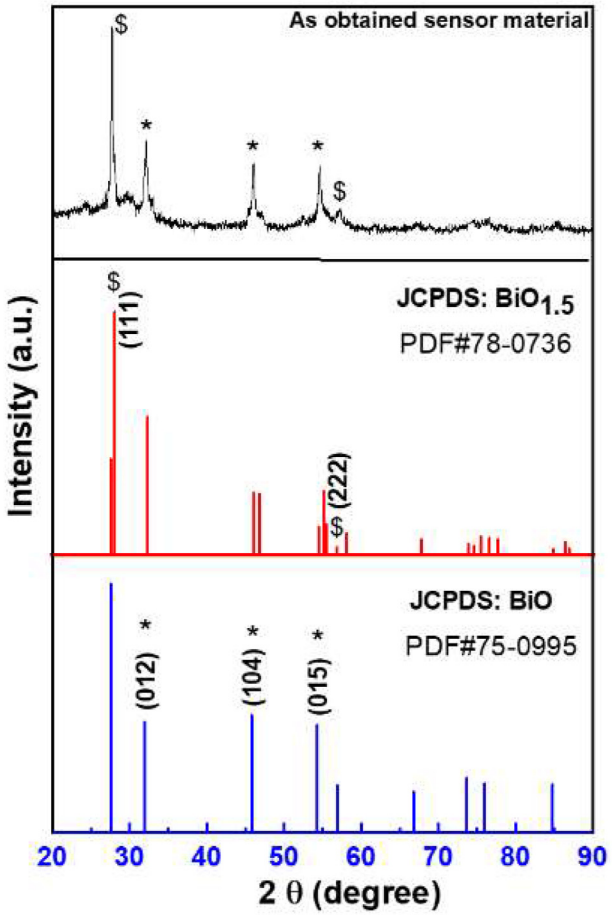

Fig. 1 – XRD pattern for BiO_x material.

in Fig. 2 a) that confirms the majority of nanosheet-like structures beside some irregular nanoparticles. The TEM images for BiO_x material at different magnifications were captured to resolve nanostructure more clearly, as in Fig. 2 b) and c). It is evident from TEM images that BiO_x forms nanosheet-like structures. There are some nanosheets stacked on one another, whereas some single nanosheets were also observed in TEM images. The nanosheets allow easy and faster charge transportation along their length [19]. The maximum nanosheet length is ~1.05 μm, whereas thickness is the order of ~22–25 nm. These long nanosheets with minimal thickness lead to a higher aspect ratio and provide a larger surface area to adsorb target gas, resulting in a higher response.

The EDS spectroscopy was used to investigate elemental composition, whereas the elemental mapping images were captured to observe the elemental distribution. The EDS spectrum of BiO_x material is shown in Fig. 3. The 'Bi' and 'O' elements were confirmed from the characteristic EDS spectrum peaks of the sensor material. The atomic and weight percentages of both elements are tabulated in the table shown as an inset of Fig. 3. The elemental mapping images for BiO_x material are shown in the inset of Fig. 3, revealing the uniform distribution of 'Bi' and 'O' elements.

UV–visible and XPS spectra analysis

UV–visible spectroscopy can be used to investigate light absorption properties and bandgap of the semiconducting nanomaterial. The UV–visible spectrum of BiO_x material is shown in Fig. 4 a). The absorbance curve rises drastically from the visible to the ultraviolet region which may be due to defects (oxygen) and the size distribution of nanosheets. The Tauc plot was plotted using UV–visible absorbance data, as shown in Fig. 4 b). The bandgap of BiO_x material was estimated (~2.4 eV) by intercept at X-axis by the line fit in the Tauc plot.

The XPS spectra for BiO_x material were recorded to investigate the chemical atomic states of the elements present in the sensor material. The XPS spectra for 'Bi' and 'O' elements are represented in Fig. 4 c) and d). The Bi 4f region has two spin-orbit components Bi $4f_{7/2}$ and Bi $4f_{5/2}$, at the binding energies 159.2 and 164.5 eV, respectively [20]. These spin-orbit components are separated by 5.3 eV energy. These appearances of Bi 4f characteristic energy levels, as indicated by XPS peaks, confirm Bi–O bond. The XPS peak at 529.2 eV is associated with lattice oxygen (O 1s) from Bi–O bond [21,22].

Temperature response and selectivity

Metal oxide-based gas sensors show different performances at different operating temperatures owing to different amounts of activation energy required for the specific type of sensing gas. The different operating temperatures also affect on adsorption of gas molecules at the sensor surface, which leads to different responses. The key role is played by the optimal operating temperature of the sensor device in determining gas sensing performance [23]. Hence, the BiO_x sensor was engaged for H_2S gas sensing at different substrate temperatures. The temperature of the sensor material decides the chemical sensing reaction rate and gas molecule adsorption. As temperature increases, the chemical reaction rate will increase, but gas adsorption gets constrained with the same. Hence it is required to find out the optimal intermediate operating temperature where both the phenomenons, *i.e.* gas adsorption and a chemical reaction, achieve the equilibrium. The optimized operating temperature for the BiO_x sensor was 250 °C using 100 ppm H_2S gas, as shown in Fig. 5 (a). It was observed that the sensor response above 250 °C decreases due to restriction on target gas molecule adsorption at the sensor's surface. The maximum sensor response is decided by the type of targeted gas and the chemical nature sensor material. The selectivity study using BiO_x sensor was carried out using different gases shown in Fig. 5 (b). The selectivity study was carried out at 100 ppm target gas concentration at 250 °C. This study reveals that the sensor has a specific affinity for H_2S gas and exhibits the highest response.

Gas response and repeatability

BiO_x sensor device was tested for H_2S gas at 100 ppm gas concentrations and operating temperatures of 250 °C as in Fig. 6 (a). The resistance response of the BiO_x sensor for H_2S

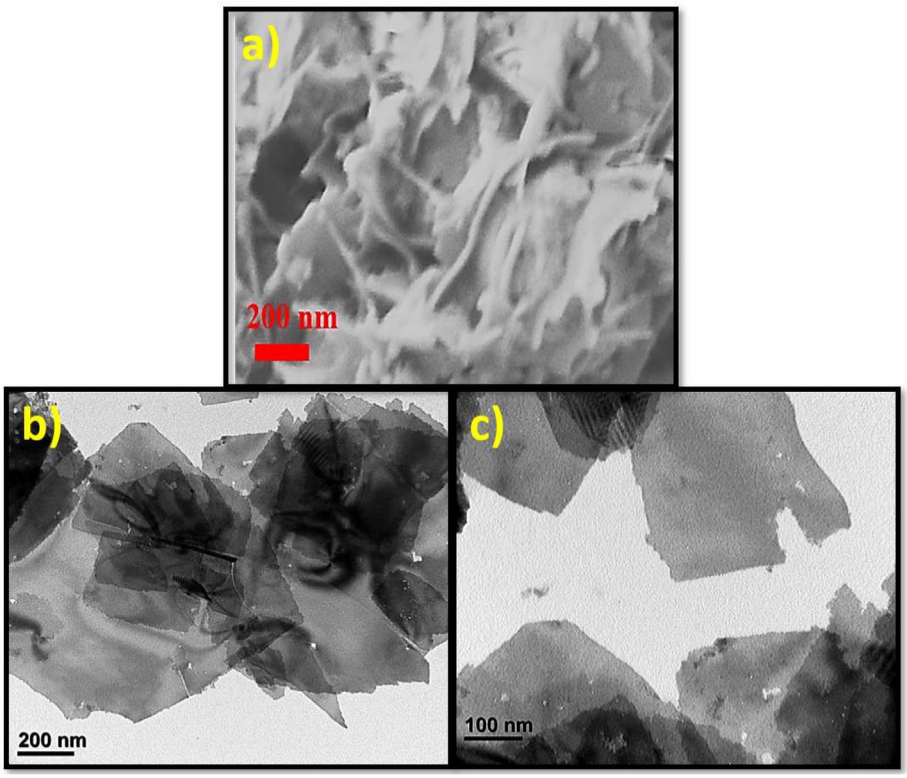

Fig. 2 – a) FESEM image, b) TEM image, c) TEM image with higher magnification for BiO_x material.

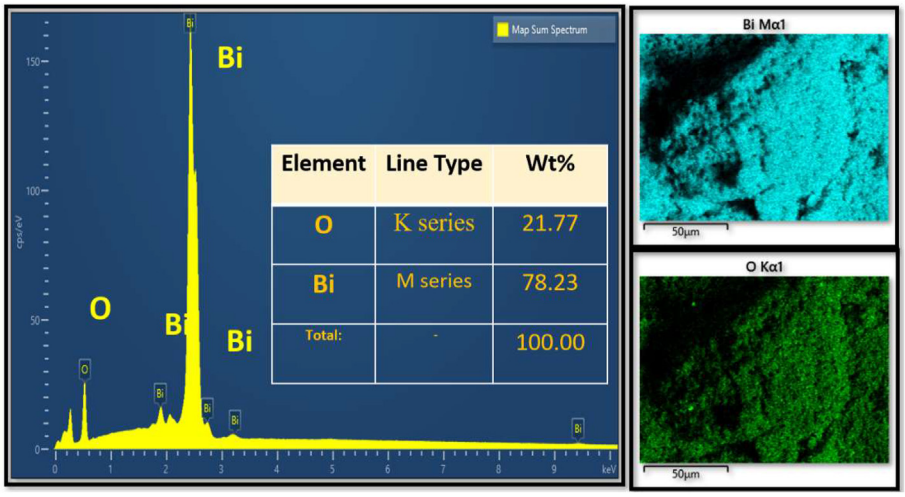

Fig. 3 – EDS, elemental mapping images, inset shows elemental composition percentage for BiO_x material.

gas was recorded as a function of time. The resistance of the BiO_x sensor decreased with the H_2S gas insertion time and increased during the recovery (target gas removal) process. The sensor's response time was the time required for attending 90% of the resistance change during gas exposure [24]. The response time of the BiO_x sensor was measured to be 511 s, whereas the recovery time was 492 s. The dynamic repeatability of the BiO_x sensor is significant in confirming the consistency of the device. The dynamic repeatability of the device for 100 ppm H_2S with continuous response and recovery was demonstrated at 250 °C, as shown in Fig. 6 (b). The sensor device offers dynamic repeatability by regaining the original resistance after every cycle of the same amount of target gas exposure, which confirms the excellent reliability of the device.

H_2S sensing mechanism

The working principle of metal oxide-based resistive type gas sensors is related to the change in resistance of the sensor during target gas exposure. This change in resistance is allied with the net concentration of targeted gas at the surface of

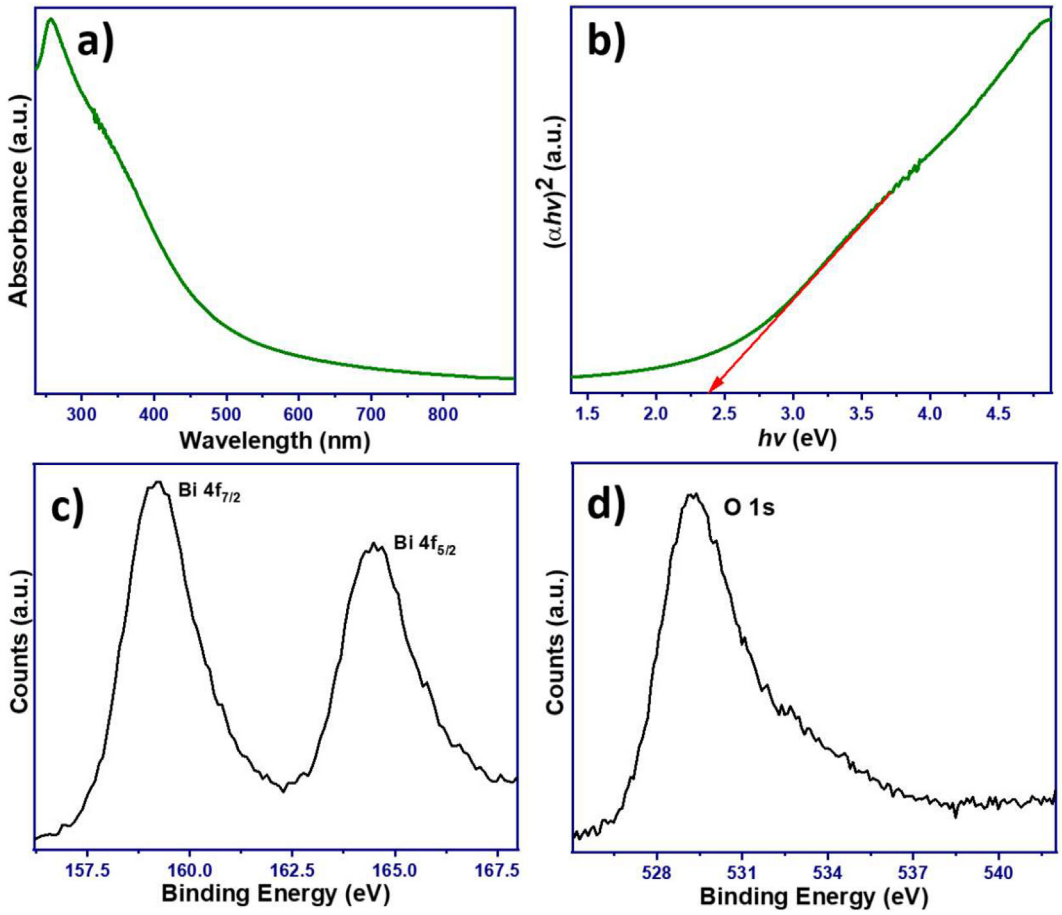

Fig. 4 – a) UV–visible absorbance, b) Tauc's plot, c) XPS spectrum associated with 'Bi', d) XPS spectrum associated with 'O' for BiO_x material.

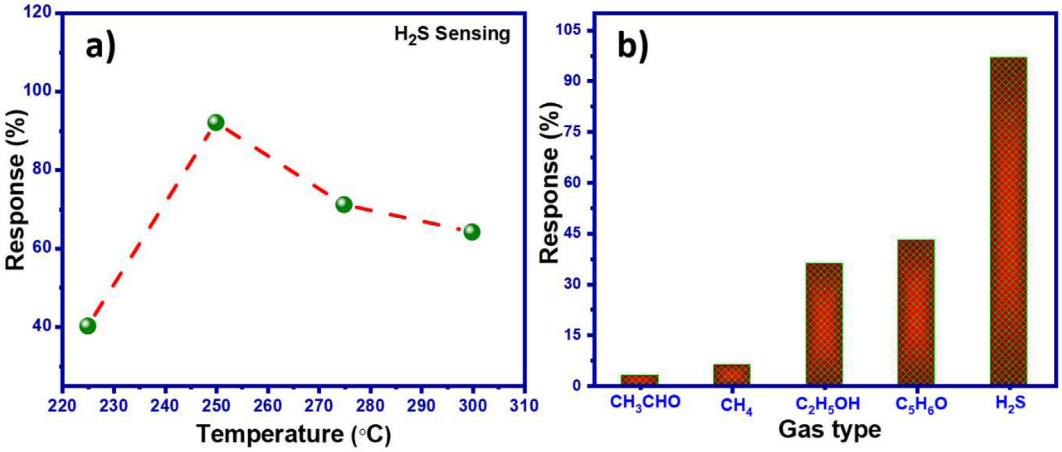

Fig. 5 – a) H_2S sensing response at different temperatures, b) selectivity study for BiO_x sensor at 100 ppm H_2S.

sensor. The chemical catalytic reaction decides the net number of charges produced or reduced at the surface of the sensor. The resistance of n-type semiconductor sensor material drops on exposure to reducing gas at its working conditions. The nanostructured bismuth oxide (BiO_x) is n-type semiconductor owing to its number of oxygen vacancies (defect), whereas H_2S is a reducing gas. Hence on exposure to H_2S gas, the resistance of BiO_x sensor drops down.

The schematic representation of the BiO_x sensor for H_2S sensing is represented in Fig. 7. The air oxygen molecules adsorb on the sensor surface and gain electrons from the conduction band of BiO_x material, forming oxygen ions. This

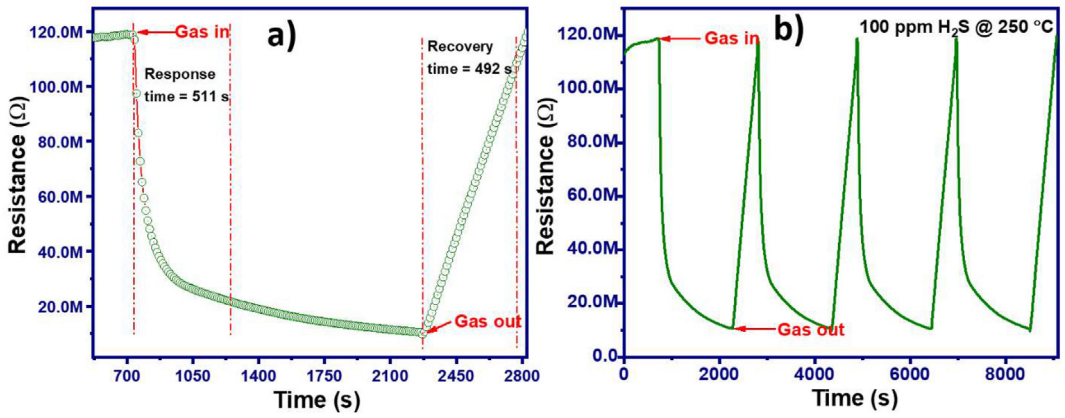

Fig. 6 – a) Transient resistance response, b) repeatability of resistance response, of BiO_x sensor for 100 ppm H_2S gas at 250 °C.

migration of electrons (from the conduction band) is responsible for the depletion region creation at the sensor surface. Two physically connected sensor particles add the depletion width across the interface, and the corresponding potential barrier φ_A is raised, which leads to an increase in the sensor's resistance, as shown in Fig. 7 a). During the sensing, H_2S gas molecules adsorb at the sensor surface and react with oxygen ions. The electron is released back to the sensor material, thereby reducing the depletion region width at the sensor's surface. The potential barrier φ_B at the interface of the two adjacent particles reduces, leading to a decrease in the sensor's resistance, as shown in Fig. 7 b). Hence the reduction in the potential barrier as well as corresponding sensor resistance contributes to the response.

Concentration effect and stability studies

The concentration effect of H_2S gas on the sensor was investigated for different concentrations from 10 to 100 ppm at 250 °C, as shown in Fig. 8(a). The figure shows the linear response at a low H_2S concentration and becomes consistent at higher concentrations. The gas response increases systematically towards different concentrations of gas. The gas response is decided by the diffusivity of the target gas molecules, and the available number of active sites on a given active surface area that decides the detection range for the target gas. The highest response of the BiO_x sensor was found to be 92% at 100 ppm H_2S concentration, whereas the lowest detection limit was 10 ppm with a gas response of 22%. The assembly design and chamber volume partially decide the lowest detection limit.

The stability of the sensor is one of the essential properties that decides the reliability and life of the sensor. Fig. 8 (b) shows the stability study for the BiO_x sensor device. The sensor was observed to be stable with minimal variation. The study was conducted over 30 days, and the response was approximately similar over the period. The performance of the BiO_x sensor was compared with the reported data on the H_2S gas sensor application, and the results are summarized in Table 1 [25–31]. It was observed from the comparison that the BiO_x sensor exhibited the highest response toward low H_2S

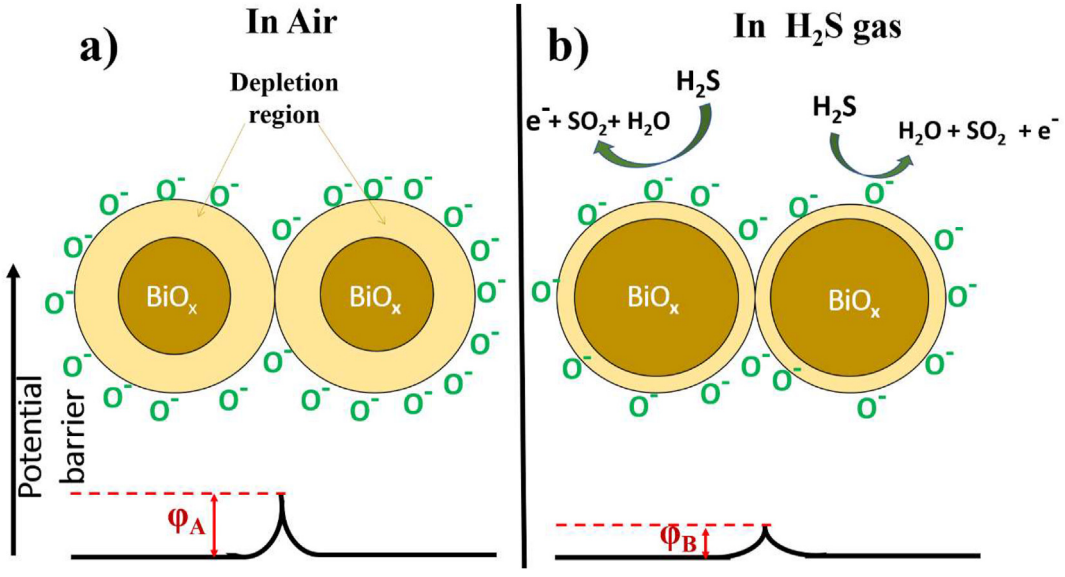

Fig. 7 – Schematic of H_2S sensing mechanism for BiO_x sensor, a) oxidation, b) reduction.

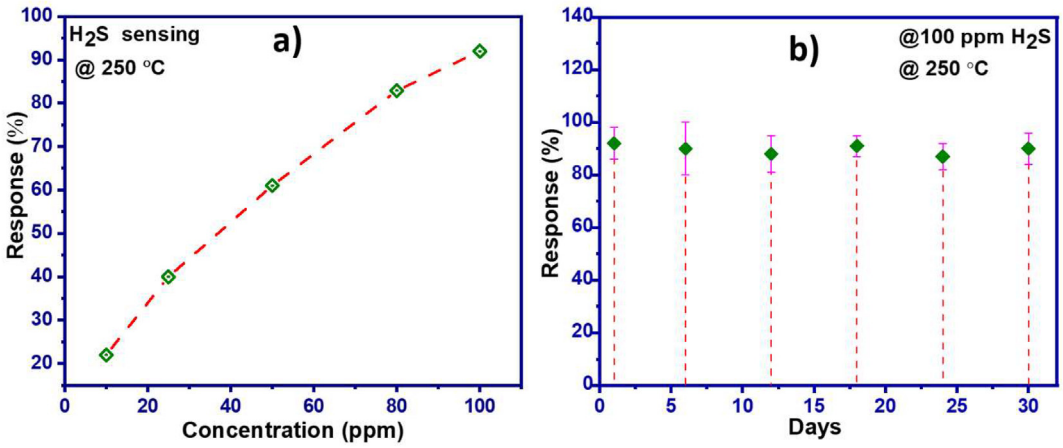

Fig. 8 – a) Response for different H_2S gas concentrations, b) stability study, for BiO_x sensor at 250 °C.

Table 1 – Comparison with reports on H_2S gas sensors with the present data.

Material	Operating temperature (C)	Gas Response (S)	Concentration (ppm)	Ref.
BiO_x	250	92%	100	This Work
CuO NRs	250	4 ($\Delta R/R_a$)	100	[25]
ZnO NRs	30	17.3 ($\Delta R/R_a$)	100	[26]
WO_3 NWs	300	1.84 (R_a/R_g)	100	[27]
CuO-functionalized WO_3 NWs	300	6.72 (R_a/R_g)	100	[27]
Co_3O_4 films	200	3.5 ($\Delta R/R_a$)	200	[28]
α-MoO_3/ZnO NCs	270	30 (R_a/R_g)	100	[29]
In-doped ZnO	250	60 (R_a/R_g)	100	[30]
CdO-decorated NiO film	92	102.5 (R_a/R_g)	100	[31]

gas concentration at a low operating temperature relatively. This high performance of the present sensor may be due to its 2-D nanosheets structure with a higher aspect ratio and the stoichiometry ($BiO_{1.5}$ and BiO) *i.e.* the mixture of two phases that may form heterojunction and number of oxygen vacancies (may serve as active sites or receptor function).

Conclusions

To sum up, we have successfully synthesized the ultra-thin nanostructured bismuth oxide using the hydrothermal route. The prepared material was characterized for structural, morphological, elemental, compositional, and chemical atomic state properties using standard tools. The prepared active material was used to fabricate gas sensor devices and tested for various gases. The sensor was tested at different temperatures and concentrations of H_2S gas. The BiO_x sensor revealed a high response of 22–92% for 10–100 ppm H_2S gas at 250 °C operating temperature. The BiO_x sensor showed high selectivity and dynamic repeatability toward 100 ppm H_2S gas at 250 °C. The plausible H_2S sensing mechanism and long-term (30 days) stability were also studied for BiO_x sensor. The larger thin nanosheet morphology of sensor material offers a high surface-to-volume ratio and the different oxygen composition provides defects that serve as active sites for gas adsorption. Hence, the nanostructured morphology and non-stoichiometry structure of BiO_x sensor material can be a promising candidate for H_2S sensor application.

Data availability

The raw/processed data required to reproduce these findings can not be shared at this time as the data also forms part of ongoing research.

Declaration of competing interest

The authors declare that they have no known competing financial interests or personal relationships that could have appeared to influence the work reported in this paper.

Acknowledgment

The author would like to thank the Vice-chancellor KBCNM University and the Principal, Yeshwant college, Nanded, India to allow the present work to publish.

Appendix A. Supplementary data

Supplementary data to this article can be found online at https://doi.org/10.1016/j.ijhydene.2022.09.235.

REFERENCES

[1] Pifferi S, Menini A. Odorant detection and discrimination in the olfactory system. Sensors and microsystems, lecture notes in electrical engineering 2011;91:3–18.
[2] Rouby C, Schaal B, Dubois D, Gervais R, Holley A. Olfaction, taste, and cognition. 1 st ed. Cambridge: Cambridge University Press; 2002.
[3] Cortes HJ, Winniford B, Luong J, Pursch M. Comprehensive two dimensional gas chromatography review. J Separ Sci 2009;32:883–904.
[4] Haddad PR, Nesterenko PN, Buchberger W. Recent developments and emerging directions in ion chromatography. J Chromatogr A 2008;1184(1):456–73.
[5] Mirzaei A, Park S, Sun GJ, Kheel H, Lee C. CO gas sensing properties of $In_4Sn_3O_{12}$ and TeO_2 composite nanoparticle sensors. J Hazard Mater 2016;305:130–8.
[6] Zhu Z, Kao CT, Wu RJ. A highly sensitive ethanol sensor based on Ag@TiO_2 nanoparticles at room temperature. Appl Surf Sci 2014;320:348–55.
[7] Pandey SK, Kim KH, Tang KT. A review of sensor-based methods for monitoring hydrogen sulfide. TrAC Trends Anal Chem (Reference Ed) 2012;32:87–99.
[8] Ashori E, Nazari F, Illas F. Adsorption of H_2S on carbonaceous materials of different dimensionality. Int J Hydrogen Energy 2014;39:6610–9.
[9] Tamaki J, Shimanoe K, Yamada Y, Yamamoto Y, Mirua N, Yamazoe N. Dilute hydrogen sulphide sensing properties of CuO-SnO_2 thin film prepared by low-pressure evaporation method. Sensor Actuator B Chem 1998;49:121–5.
[10] Mortezaali A, Moradi R. The correlation between the substrate temperature and morphological ZnO nanostructures for H_2S gas sensors. Sensor Actuator Phys 2014;206:30–4.
[11] Nakate UT, Yeon-Tae Yu, Park S. Hierarchical CuO nanostructured materials for acetaldehyde sensor application. Microelectron Eng 2022;251:111662.
[12] Balouria V, Kumar A, Samanta S, Singha A, Debnath AK, Mahajan A, Bedi RK, Aswal DK, Gupta SK. Nano-crystalline Fe_2O_3 thin films for ppm level detection of H_2S. Sensor Actuator B Chem 2013;181:471–8.
[13] Nakate UT, Yeon-Tae Yu, Park Sungjune. Hydrothermal synthesis of ZnO nanoflakes composed of fine nanoparticles for H_2S gas sensing application. Ceram Int 2022;48(19):28822–9. https://doi.org/10.1016/j.ceramint.2022.03.017.
[14] Wang J, Chen J, Liu F, Jia M, Zhang Z, Liu M, Jiang L. Renewable WO_3/Bi_2O_3 heterojunction for photoelectrochemical and visual dual-mode detection of hydrogen sulfide. Sensor Actuator B Chem 2022;369:132274.
[15] Zhang F, Zheng M, Zhang X, Cheng X, Li M, Huo L, Zhou X, Xu Y. Rapid detection of H_2S gas driven by the catalysis of flower-like α-$Bi_2Mo_3O_{12}$ and its visual performance: a combined experimental and theoretical study. J Hazard Mater 2022;424:127734.
[16] Kadam SL, Ingole RS, Tiwari NG, Nakate UT, Nakate YT, Kulkarni SB. Role of deposition temperature on physical and electrochemical performance of manganese oxide electrode material for supercapacitor application. Mater Sci Eng, B 2022;285:115934.
[17] Nakate UT, Ahmad R, Patil P, Yu YT, Hahn YB. Ultra thin NiO nanosheets for high performance hydrogen gas sensor device. Appl Surf Sci 2020;506:144971.
[18] Nakate UT, Bhuyan P, Yu YT, Park S. Synthesis and characterizations of highly responsive H_2S sensor using p-type Co_3O_4 nanoparticles/nanorods mixed nanostructures. Int J Hydrogen Energy 2022;47(12):8145–54.
[19] Nakate UT, Yu YT, Park S. High performance acetaldehyde gas sensor based on pn heterojunction interface of NiO nanosheets and WO_3 nanorods. Sensor Actuator B Chem 2021;344:130264.
[20] Arshad H, Tahir MU, Rehman F, Wang L, Wang J, Su X, Yang C. Facile synthesis of bismuth oxide nanostructures derived from solvent-mediated oxalates and their visible-light-driven photocatalytic removal of organic pollutants. Appl. Sur. Sci. 2022;574:151678.
[21] Köhler R, Siebert D, Kochanneck L, Ohms G, Viöl W. Bismuth oxide faceted structures as a photocatalyst produced using an atmospheric pressure plasma jet. Catalysts 2019;9(6):533.
[22] Narwade SH, Shinde PV, Shinde NM, Jadhav VV, Shaikh SF, Mane RS, Bhosle UV. Hydrangea-type bismuth molybdate as a room-temperature smoke and humidity sensor. Sensor Actuator B Chem 2021;348:130643.
[23] Waghmare SD, Jadhav VV, Shaikh SF, Mane RS, Rhee JH, O'Dwyer C. Sprayed tungsten-doped and undoped bismuth ferrite nanostructured films for reducing and oxidizing gas sensor applications. Sensor Actuator Phys 2018;271:37–43.
[24] Ghule BG, Shinde NM, Raut SD, Shaikh SF, Al-Enizi AM, Kim KH, Mane RS. Porous metal-graphene oxide nanocomposite sensors with high ammonia detectability. J Colloid Interface Sci 2021;589:401–10.
[25] Kim H, Jin C, Park S, Kim S, Lee C. H_2S gas sensing properties of bare and Pdfunctionalized CuO nanorods. Sensor Actuator B Chem 2012;161:594–9.
[26] Zhang N, Yu K, Li Q, Zhu ZQ, Wan Q. Room-temperature high sensitivity H_2S gas sensor based on dendritic ZnO nanostructure with macroscale in appearance. J Appl Phys 2008;103:104305.
[27] Park S, Park S, Jung J, Hong T, Lee S, Kim HW, Lee C. H_2S gas sensing properties of CuO-functionalized WO_3 nanowires. Ceram Int 2014;40:11051–6.
[28] Navale ST, Liu C, Gaikar PS, Patil VB, Sagar RUR, Du B, Manee RS, Stadler FJ. Solution-processed rapid synthesis strategy of Co_3O_4 for the sensitive and selective detection of H_2S. Sensor Actuator B Chem 2017;245:524–32.
[29] Yu HL, Li L, Gao X-M, Zhang Y, Meng F, Wang TS, Xiao G, Chen YJ, Zhu C-L. Synthesis and H_2S gas sensing properties of cage-like MoO_3/ZnO composite. Sensor Actuator B Chem 2012;171:679–85.
[30] Badadhe SS, Mulla IS. H_2S gas sensitive indium-doped ZnO thin films: preparation and characterization. Sensor Actuator B Chem 2009;143:164–70.
[31] Yu TT, Zhang XF, Xu YM, Cheng XL, Gao S, Zhao H, Huo LH. Low concentration H_2S detection of CdO-decorated hierarchically mesoporous NiO nanofilm with wrinkle structure. Sensor Actuator B Chem 2016;230:706–13.